Journal of Materials Chemistry A

Accepted Manuscript

ROYAL SOCIETY OF CHEMISTRY

www.rsc.org/materialsA

Journal Name COMMUNICATION

Hysteresis-free Multi-wall Carbon Nanotube-based Perovskite Solar Cells with a High Fill Factor

Zhanhua Wei, Haining Chen, Keyou Yan, Xiaoli Zheng and Shihe Yang*

Received 00th January 20xx,
Accepted 00th January 20xx

DOI: 10.1039/x0xx00000x

www.rsc.org/

Abstract: Among the various perovskite solar cells, the carbon-based hole-transporter-free type is arguably the most promising for applications because of its low materials/manufacturing cost, high efficiency and the best long-term stability. However, the fill factor (FF) is typically below 0.75, limiting the cell performance. In this communication, through systematic performance comparision between multi-wall carbon nanotube (MWCNT) and another two representative carbon materials, namely carbon black and graphite, we highlight two salient advantages for MWCNT-bsed devices: high FF and hysteresis-free performance. We owe the superior performance to the charge transport highway at the interface of MWCNT/perovskite. After preliminary optimization, we have achieved a PCE of 12.67 % with a very impressive FF of 0.80, which is among the highest for carbon-based perovskite solar cells.

Recently, the continuous and rapid development of the organometal halide perovskite solar cells has attracted much attention not only from research laboratory but also photovoltaic industry. The perovskite solar cells are famous for their fantastic power conversion efficiency (PCE) gain (up to a certified value of 20.1 %) and the solution-processable fabrication process.[1-3] Among the various kinds of perovskite solar cell structures, including mesoscopic, planar and inverted designs,[4-7] the most common and successful ones can be expressed as TiO_2/perovskite/hole-transporter/Au. However, as the most commonly used hole transporter material (HTM), spiro-OMeTAD has proved to be non-stable in air to say nothing about its long-term stability.[8-11]

To improve the long-term cell stability, some stable inorganic HTMs, such as CuSCN,[12, 13] were used to replace with the spiro-OMeTAD and have shown a PCE of 12.4 %. Even more radical, Au electrode was deposited on perovskite without the spiro-OMeTAD interlayer and a PCE of 11.5 % was still achieved.[14-16] Viewing from many facets of cost, performance, stability and manufacturing simplicity, carbon-based HTM-free perovskite solar cells have proved to be one of the most promising perovskite solar cells. In such perovskite solar cells (shown in Figure 1A), electrons are injected from perovskite to TiO_2 and finally collected by FTO. Meanwhile, holes are extracted from perovskite to carbon electrode directly, eliminating both noble metal electrode and HTM. Here one of the key processes is hole extraction at the interface of carbon/perovskite, the quality of which is strongly influenced by interface engineering strategy,[17-19] carbon material type,[20] particle size/shape[21, 22] and electronic property.[22, 23] Typically, the FF of nanocarbon-based perovskite solar cells is <0.75 (shown in Table S1),[17, 22, 24, 25] which is substantially lower than that of the state-of-art HTM-based devices, e.g., >0.78.[1, 2] Compellingly, carbon nanotubes should make an excellent hole extraction electrode material owing to their extraordinary electrical, thermal, mechanical, electrical and net-work forming properties.[26, 27] To our knowledge, however, there has been no study in this direction due to the challenges of proper carbon/perovskite interface engineering.

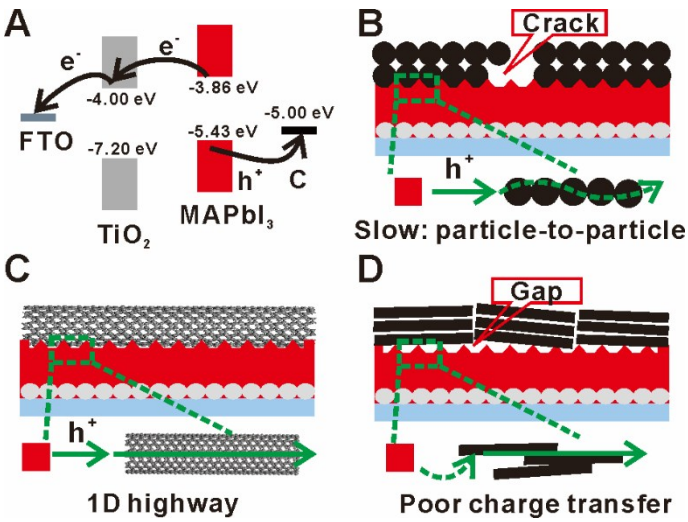

Figure 1. (A) Energy level diagram of the nanocarbon-based hole-transporter-free perovskite solar cells. Schematic diagram of cell architecture and hole extraction process of three carbon-based perovskite solar cells fabricated with different carbon materials: (B) Carbon black, (C) MWCNT and (D) Graphite flake (the green and solid arrows indicate effective and fast transport, while the green and dashed arrows denote poor pathways).

Herein, we report a multi-wall carbon nanotube (MWCNT, 773840 ALDRICH, ≥98% carbon basis, O.D. × I.D. × L 10 nm ± 1 nm × 4.5 nm ± 0.5 nm × 3~6 μm) electrode, its seamless interface with a perovskite layer achieved by the chemical reaction embedment technique we reported previously,[17-19, 28] and the integration of the electrode and the interface into an efficient carbon-based perovskite solar cell. For direct comparison, two other representative carbon materials

Department of Chemistry, The Hong Kong University of Science and Technology, Clear Water Bay, Kowloon, Hong Kong, China
[*] Corresponding author: chsyang@ust.hk
[**] This work was supported by the HK Innovation and Technology Fund (ITS/004/14) and the HK-RGC General Research Funds (GRE No. HKUST 606511).
Electronic Supplementary Information (ESI) available: Experimental details and Figure S1 – S13. See DOI: 10.1039/x0xx00000x

(carbon black and graphite, see ESI for more details) were also used to fabricate solar cells in the same way (for experimental details, please refer to ESI, Figure S1). It turns out that the MWCNT electrode is superior to the other carbon electrodes in terms of a much higher FF due to their more robust interface.

In brief, a compact and mesoscopic TiO_2 thin film was prepared by one-step $TiCl_4$ treatment firstly (shown in Figure S2). Then, the PbI_2 thin film and the three carbon thin films were deposited in sequence by spin-coating and drop-casting, respectively. At last, 100 μL of a CH_3NH_3I solution (IPA, 10 mg mL^{-1}) was dropped onto the above FTO/TiO_2/PbI_2/C substrates for 3 min, dried by spinning and heated at 100 °C for 10 min. This step involves the so-called *in-situ* chemical reaction embedment which ensures the seamless contact of the C/perovskite interface in an evaporative wet medium.

It can be seen from the ultraviolet photoelectron spectra (UPS, shown in Figure S3) that the above three carbon materials have a similar work function. As a result, the corresponding perovskite solar cells have the same energy level alignment relative to perovskite (Figure 1A).

A full hole extraction comprises two major steps: one is hole extraction from perovskite to C nanoparticle and the other is charge transport through the C film. With the chemical reaction embedment strategy, the carbon materials can be seamlessly connected with the perovskite film, forming a high quality carbon/perovskite interface that allows fluent hole extraction from perovskite to carbon. This is clearly manifested in Figure 1B for C black particles. However, the carbon black film is easily cracked due to lack of binding force. In this case, transport of the extracted holes from particle-to-particle through the carbon black film is expected to be slow.

As regards the MWCNT electrode shown in Figure 1C, a seamless interface between the MWCNTs and the perovskite is also formed with the chemical embedment technique, securing an efficient interfacial hole extraction process. What's unique here is that the MWCNT network can work as charge transfer highway for holes and should be beneficial to photovoltaic performance, which will be discussed below. Another extreme case is the graphite flake electrode shown in Figure 1D. Although charge transport through the graphite flake film is expected to be fast, the hole extraction from the perovskite to the graphite flakes is encumbered simply because the graphite flakes are too large in size and cannot form a good contact with the perovskite crystalline film.

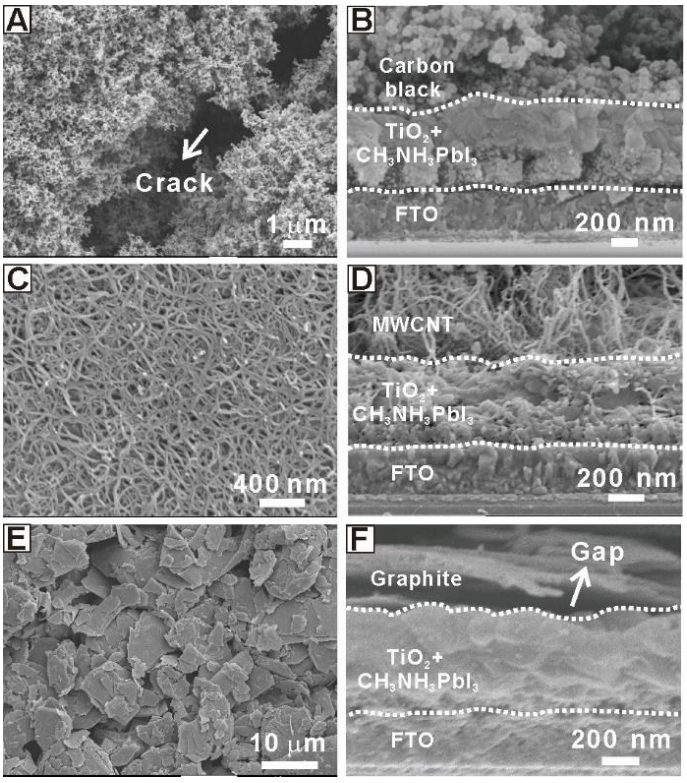

Figure 2. (A, C, E) Top view and (B, D, F) cross-sectional SEM images of the carbon black, MWCNT and graphite-based perovskite solar cells. The dashed lines in (B, D, F) represent the interface of FTO/TiO_2 and $CH_3NH_3PbI_3$/C, respectively.

As mentioned above, the morphology of carbon materials has great influence on the interface quality of carbon/perovskite and then solar cell performance. To closely examine the morphology difference, we turned to use scanning electron microscope (SEM) to observe the carbon thin film and interface of carbon/perovskite. Figure 2A shows the top view SEM image of a carbon black thin film, which is loosely packed by ~ 30 nm carbon nanoparticles. As there is not binder between carbon nanoparticles and the Van der Waals force is not strong enough to make particles pack closely, the as-deposited carbon black thin film is easily to crack. In this case, the extracted holes need to be transported from one particle to the surrounding particle, which is supposed to be not a so efficient way. And the cracks on carbon thin film is thought to be harmful to photovoltaic performance.[21] As for the interface of carbon black/perovskite, shown in Figure 2B, we can see a ~ 650 nm of TiO_2/$CH_3NH_3PbI_3$ composite layer is seamlessly connected with carbon black thin film. From transmittance electron microscope (TEM) images of MWCNT shown in Figure S4, it can be seen that the MWCNT is a 1-dimensional material with ~ 15 nm in diameter and several micrometres long. The long chain-like structure make MWCNT easily pack and cross together to form a continuous and crack-free thin film (shown in Figure 2C). Similar to carbon black, with chemical embedment technique, the MWCNT can also be strongly attached on the perovskite thin film (shown in Figure 2D and Figure S5). As shown in Figure 2E, the graphite thin film consists of 2-demensional (2D)

flakes which are on the scale of tens of micrometres, significantly bigger than the carbon black particles and MWCNTs. Thanks to the 2D flake structure, the graphite flakes tend to pack compactly and connect with each other forming a continuous thin film. However, as the graphite flakes are too large in size and too rigid to fold, the as-deposited graphite thin film cannot fully contact the PbI_2 thin film, leaving behind many gaps between the perovskite and graphite films even after chemical embedment (shown in Figure 2F). It is believed that the gaps will bring in severe charge transfer problems and result in poor photovoltaic performance, which will be discussed below.

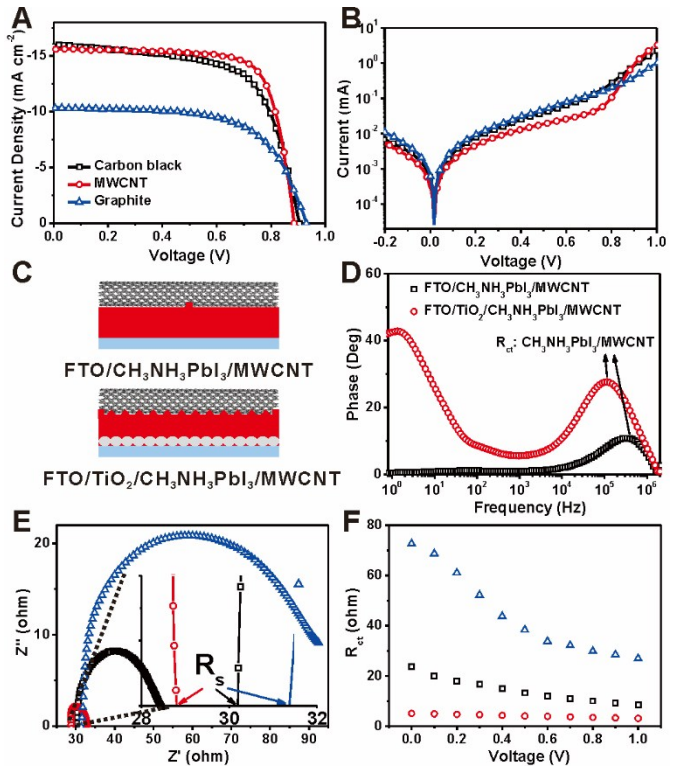

Figure 3. (A) *J-V* curves under 1 sun illumination and (B) dark *I-V* curves (semilog plot, cell area: 0.2 cm^2) of the as-fabricated three carbon-based perovskite solar cells. (C) Schematic diagrams and (D) EIS spectra (Bode phase plots, bias: 0 V) of two model devices with the configuration of $FTO/CH_3NH_3PbI_3/MWCNT$ and $FTO/TiO_2/CH_3NH_3PbI_3/MWCNT$ (frequency: 4 MHz to 100 mHz). (E) EIS spectra (Nyquist plot, bias: 0 V) and (F) derived R_{ct} as a function of applied voltage of the three model devices with the configuration of $CH_3NH_3PbI_3/C$ (frequency: 4 MHz to 1 kHz). All the EIS experiments were conducted under 1 sun condition.

To evaluate the photovoltaic performance of the as-fabricated three carbon-based perovskite solar cells, current-voltage (*J-V*) characteristics under 1 sun condition and dark *J-V* were recorded and presented in Figure 3A and 3B. From Figure 3A and Table 1, it is obviously that the graphite device shows a high open-circuit voltage (V_{oc}) of 0.93 V, fill factor (FF) of 0.64, but the lowest current density (J_{sc}) of 10.30 mA cm^{-2} and only yielding a PCE of 6.13 %. The apparent low J_{sc} should be attributed to the poor contact between graphite film and perovskite film (due to gaps as indicated in Figure 2F). While, the carbon black device shows a significantly higher J_{sc} of 15.98 mA cm^{-2}, together with a V_{oc} of 0.90 V, FF of 0.65 and corresponding PCE of 9.35 %. As for the MWCNT device, the most impressive aspect is the high FF of as high as 0.75, accompanied by a V_{oc} of 0.88 V and a J_{sc} of 15.60 mA cm^{-2}, resulting a PCE of 10.30 %. One of the reasons for the high FF is related to the superior conductivity (shown in Figure S6). Specifically, the conductivity of MWCNT is 35.60 S cm^{-1}, which is 4.30 times higher than graphite and 7.43 times higher than carbon black. In common parlance, the FF is sensitive to the interface quality and directly correlated with the shunt resistance (R_{sh}) and the series resistance (R_s). The values of R_{sh} and R_s are extracted from the *J-V* curves and shown in Table S1. It can be seen that the MWCNT device has the lowest R_s but the highest R_{sh}, significantly higher, indicating a more fluent hole extraction and larger recombination suppression at the interface of $CH_3NH_3PbI_3$/MWCNT. From the cell efficiency statistic results shown in Figure S7, one can see that the MWCNT device's performance is significantly higher than the carbon black and graphite devices.

Table 1. Solar cell parameters of the three as-fabricated carbon-based perovskite solar cells.

Solar cells	V_{oc} (V)	J_{sc} (mA cm^{-2})	FF	PCE (%)
Carbon black	0.90	15.98	0.65	9.35
MWCNT	0.88	15.60	0.75	10.30
Graphite	0.93	10.30	0.64	6.13

In addition, the dark *J-V* curves also provide valuable information, such as R_s, R_{sh} and leakage current.[4, 29] From the dark *J-V* curves shown in Figure 3B, it can be seen that the dark current of the MWCNT device under reverse bias is significantly lower than that of carbon black and graphite devices, suggesting that the MWCNT device shows the lowest leakage current. Moreover, in the forward bias region after 0.85 V, the injected current density of the MWCNT device is much higher than the other two devices, revealing a lower injection barrier between the MWCNT and perovskite. As all of the three carbon-based perovskite devices have the similar $TiO_2/CH_3NH_3PbI_3$ interface and the similar $CH_3NH_3PbI_3$ layer, it is believed that the leakage current is mainly determined by the $C/CH_3NH_3PbI_3$ interface quality. By comparison, the leakage current is in the order of MWCNT < carbon black < graphite, and the charge injection barrier is in the order of MWCNT < carbon black < graphite too, suggesting that the interface quality of $C/CH_3NH_3PbI_3$ is in the order of MWCNT > carbon black > graphite. In other words, the superior conductivity of the MWCNT network and the high quality of the MWCNT/$CH_3NH_3PbI_3$ interface are primarily responsible for the remarkable increase of FF.

Electrochemical impedance spectra (EIS) of some model devices were recorded and used to analyse the interfacial charge transfer and recombination processes. As shown in Figure 3C, we fabricated two model devices with the architecture of $FTO/CH_3NH_3PbI_3/MWCNT$ and $FTO/TiO_2/CH_3NH_3PbI_3/MWCNT$, respectively. Figure 3D shows the Bode phase plots, and there is only one peak in the high

frequency region (4 MHz to 1 kHz) for the FTO/$CH_3NH_3PbI_3$/MWCNT device. By contrast, the FTO/TiO_2/$CH_3NH_3PbI_3$/MWCNT devices shows one peak in the high frequency region and another peak in the low frequency region (<10 Hz). Based on these results and some literature,[30] we can attribute the high frequency peak to the charge transfer process for the interface of $CH_3NH_3PbI_3$/MWCNT and the low frequency peak to the overall charge recombination process in the perovskite thin film. As all of the as-fabricated three carbon-based perovskite devices have the similar TiO_2/$CH_3NH_3PbI_3$ interface, it is believed that the different charge transfer process of the $CH_3NH_3PbI_3$/C interface should be responsible for the PCE difference. Figure 3E shows the Nyquist plots of the three kinds of perovskite model devices with the configuration of $CH_3NH_3PbI_3$/C (frequency from 4 MHz to 1 kHz, bias: 0V). In Figure 3E, for each device, only one semi-circle is observed, which represent the charge transfer resistance (R_{ct}) of $CH_3NH_3PbI_3$/C interface. It can be seen that the MWCNT device has the lowest R_s and R_{ct}. Figure 3F presents the curve of derived R_{ct} as a function of applied voltage (the original data and equivalent circuit are shown in Figure S8), it can be seen that R_{ct} is in the order of MWCNT < carbon black < graphite at all applied voltage range. By combining *J-V* test and EIS result, we can conclude that the superior performance of MWCNT devices should be attributed to the ultra-small R_s and R_{ct}.

Despite the widely known high efficiencies,[1, 2] perovskite solar cells still suffer from hysteresis effect, which is dependent on scan direction and scan rate.[31, 32] Such hysteresis effect seriously causes cell stability concern and difficulty to accurately determine the cell efficiency. To investigate photocurrent hysteresis effect of the as-fabricated three carbon-based perovskite solar cells, *J-V* curves with different scan direction (forward: from 0 V to 1 V, backward: from 1 V to 0V) and scan rate (10 mV s^{-1}, 50 mV s^{-1} and 100 mV s^{-1}) were recorded and presented in Figure 4. For clearly describe the difference between the efficiency of forward scan and backward scan, we define a difference factor according to the following equation:

$$Difference\ factor = \frac{\eta_{Backward} - \eta_{Forward}}{\eta_{Backward}}$$

Where $\eta_{Backward}$ and $\eta_{Forward}$ are corresponding to the PCE of the backward scan and forward scan respectively.

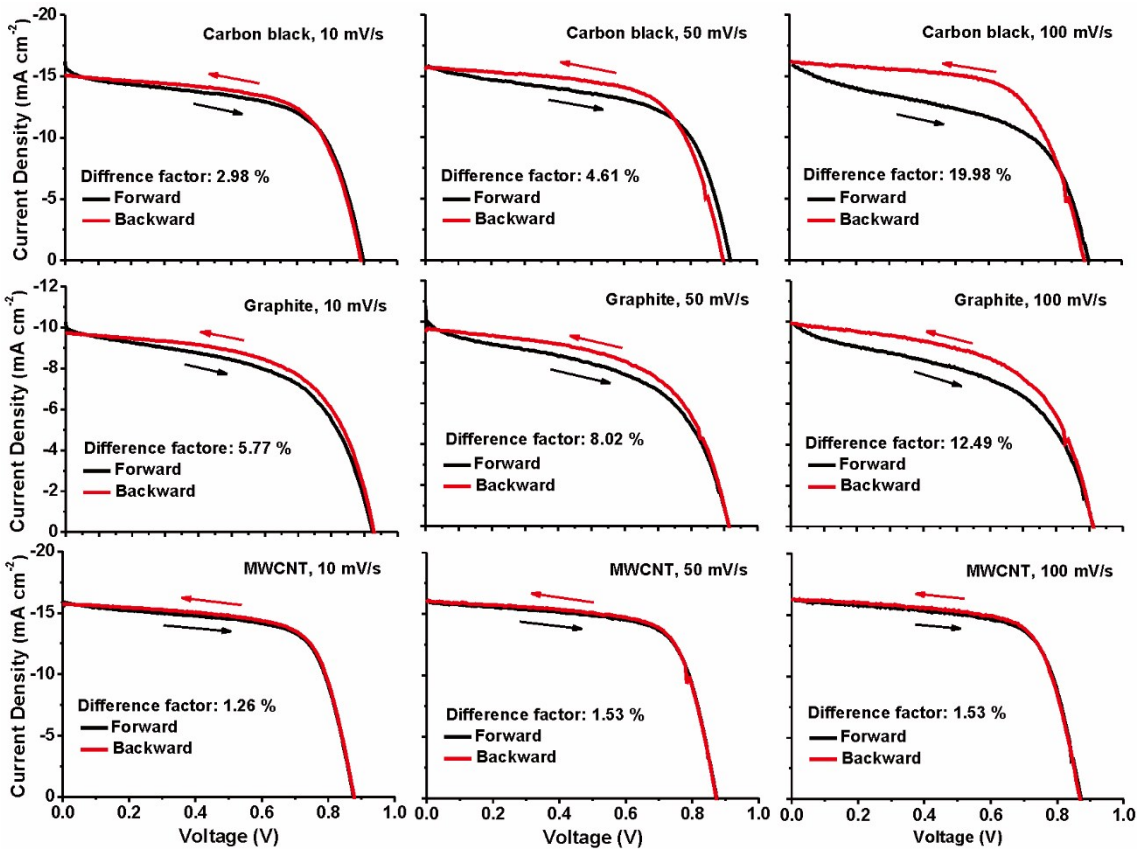

Figure 4. Hysteresis effect investigation of the as-fabricated three carbon-based perovskite solar cells: carbon black, graphite and MWCNT.

As shown in Figure 4, at a scan rate of 10 mV s^{-1}, the forward and backward curves of carbon black and MWCNT devices nearly overlap perfectly with difference factor of only 2.98 % and 1.26 % respectively, which means little hysteresis effect exist. However, the difference between forward and backward scans of graphite device is more obvious with a difference factor of 5.77 %, which means there is indeed hysteresis effect. When the scan rate increases up to 50 mV s^{-1}, the difference

factor of carbon black and graphite grow to 4.61 % and 8.02 %, respectively. While, the difference factor of MWCNT device is only 1.53 %. When the scan rate further rises to 100 mV s^{-1}, the hysteresis effect become worse for carbon black and graphite devices with a large difference factor of 19.98 % and 12.49 %, respectively. Impressively, even at this high scan rate (100 mV s^{-1}), MWCNT device only shows a difference factor of 1.53 %, which is nearly the same to the values of slow scan rate (50 mV s^{-1} and 10 mV s^{-1}). Based on the above result, we can conclude that there is no obvious hysteresis effect for MWCNT device. Moreover, the statistic result of difference factor (Figure S9) and the fast current response upon chopped illumination (Figure S10) also supports the hysteresis-free performance. However, there indeed exists significant hysteresis effect for carbon black and graphite devices. As these three carbon-based perovskite solar cells have similar cell configuration and $TiO_2/CH_3NH_3PbI_3$ interface, it is believed that the different performance on hysteresis effect is due to different interface quality of $C/CH_3NH_3PbI_3$ and the corresponding hole transfer process. By combining the EIS result in Figure 3 and hysteresis effect investigation in Figure 4, we believe that the MWCNT films can indeed serve as a charge transport highway (as indicated in Figure 1C) for the extracted holes, and this is the main reason for the higher PCE and the elimination of the hysteresis effect.

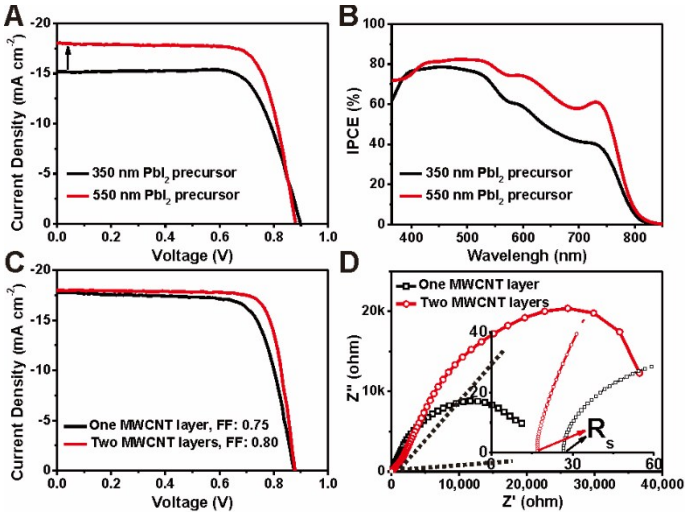

Figure 5. Cell performance optimization by increasing the PbI_2 precursor layer thickness: (A) *J-V* curves and (B) IPCE curves of devices with different PbI_2 precursor layer thicknesses. Cell performance optimization by thickening the MWCNT electrode layer (decreasing R_s): (C) *J-V* curves and (D) EIS spectra of devices with different MWCNT electrodes. EIS spectra are recorded with a bias of -0.4 V and in the dark.

On the basis of the above discussion, one can conclude that there are mainly two features for MWCNT-based perovskite device: i.e., high FF and hysteresis-free performance, which make MWCNT films a very promising hole extraction electrode material in HTM-free perovskite solar cells. It is noticed that the key limitation for the cell performance is the low J_{sc}, which is strongly dependent on perovskite composite, film thickness and quality.[2] Hence, we tried to increase the PbI_2 precursor layer thickness by multiple spin coating and increase PbI_2 solution concentration (please refer to step 2 for experimental details in ESI). As a result, the thicker PbI_2 precursor layer will result in thicker $CH_3NH_3PbI_3$ layer and higher J_{sc}. Figure 5A shows the *J-V* curves of the MWCNT-based devices fabricated with different PbI_2 precursor layer (cross-sectional SEM images are shown in Figure S11). As expected, the device fabricated with 550 nm PbI_2 precursor layer gives a higher J_{sc} (18.02 mA cm^{-2}) than the 350 nm PbI_2 layer device (15.18 mA cm^{-2}). However, even after optimization, J_{sc} of the device fabricated from the 550 nm PbI_2 layer is still lower than those reported in the literature,[1-3] probably because the PbI_2 layer is too thick and cannot be fully converted to perovskite. Considering that the perovskite layer is covered by a thick MWCNT thin film and cannot be directly tested by XRD, we prepared a perovskite thin film with the identical procedure but leaving out the MWCNT layer. As shown in Figure S12, some PbI_2 residues still can be detected in that film, which could be responsible for the low J_{sc}. Figure 5B presents the corresponding incident photon-to-current conversion efficiency (IPCE) spectrum. And an integration of the IPCE spectrum with the AM 1.5G solar photon flux yields a current density of 14.64 and 17.75 mA cm^{-2}, which are well consistent with *J-V* test result. What more, it can be seen from the IPCE spectra that the J_{sc} enhancement is mainly due to the light harvesting improvement after 550 nm. Beside J_{sc} growth, it is also found that the FF can be further increased by thickening MWCNT electrode thickness. As shown in Figure 5C, two MWCNT layers (~40 μm) device presents V_{oc} of 0.88 V, J_{sc} of 18.00 mA cm^{-2}, and very impressive FF of 0.80, yielding a PCE of 12.67 %. By contrast, one MWCNT layer (~15 μm) device show V_{oc} of 0.88 V, J_{sc} of 17.75 mA cm^{-2}, and FF of 0.75, yielding a PCE of 11.72 %. From the corresponding EIS spectra (Figure 5D, recorded in the dark with a bias of -0.4 V), the higher FF of the two MWCNT layer device should be attributed to the smaller R_s and the larger recombination resistance (R_{rec}). Further, the larger R_{rec} implicates a stronger suppression of charge recombination in the whole perovskite thin film, including the $C/CH_3NH_3PbI_3$ and $TiO_2/CH_3NH_3PbI_3$ interfaces. We have also tested the stability of one of the MWCNT devices, and the result is presented in Figure S13. One can see that the device retained ~90 % of its initial efficiency after 10 days.

Conclusions

To sum up, we have identified the MWCNTs as a superior hole extraction electrode material in HTM-free perovskite solar cells. Through systematic performance comparison between MWCNT and other two representative carbon materials (carbon black and graphite), we arrive at two reasons for the good performance of the MWCNT-based devices. The first reason is the proper size (~ 15 nm in diameter) and 1D chain structure. It is the small size that ensures the appropriate embedment of the MWCNTs into the perovskite film, while the 1D chain structure allows interpenetration to form a continuous, highly conductive and crack-free network film. The second reason is the interpenetrating charge transfer bi-continuous highway at the interface between the $CH_3NH_3PbI_3$ and the MWCNT network,

which is mainly responsible for the high FF and hysteresis-free performance. After preliminary optimization, we are able to achieve a hysteresis-free PCE of 12.67 % with a very impressive FF of 0.80. Our work opens up a new opportunity for nanocarbon-based perovskite solar cells by designing and assembling low-dimensional nanostructured and highly conductive carbon cathodes. Future work on the MWCNT-based PSC devices should focus on the improvement of J_{sc} by judiciously promoting crystalline quality of the perovskite active layer.[1, 2]

Notes and references

1 1.W. S. Yang, J. H. Noh, N. J. Jeon, Y. C. Kim, S. Ryu, J. Seo and S. I. Seok, *Science*, 2015, **348**, 1234-1237.
2 2.N. J. Jeon, J. H. Noh, W. S. Yang, Y. C. Kim, S. Ryu, J. Seo and S. I. Seok, *Nature*, 2015, **517**, 476-480.
3 3.J. Burschka, N. Pellet, S. J. Moon, R. Humphry-Baker, P. Gao, M. K. Nazeeruddin and M. Gratzel, *Nature*, 2013, **499**, 316-318.
4 4.Q. Wang, Y. C. Shao, Q. F. Dong, Z. G. Xiao, Y. B. Yuan and J. S. Huang, *Energy & Environmental Science*, 2014, **7**, 2359-2365.
5 5.Z. Xiao, Q. Dong, C. Bi, Y. Shao, Y. Yuan and J. Huang, *Adv Mater*, 2014, **26**, 6503-6509.
6 6.A. Abrusci, S. D. Stranks, P. Docampo, H. L. Yip, A. K. Y. Jen and H. J. Snaith, *Nano Letters*, 2013, **13**, 3124-3128.
7 7.J. H. Kim, P. W. Liang, S. T. Williams, N. Cho, C. C. Chueh, M. S. Glaz, D. S. Ginger and A. K. Jen, *Adv Mater*, 2015, **27**, 695-701.
8 8.J. Liu, W. Yongzhen, C. Qin, X. Yang, T. Yasuda, A. Islam, K. Zhang, W. Peng, L. Han and W. Chen, *Energy & Environmental Science*, 2014, **7**, 2963-2967.
9 9.N. J. Jeon, H. G. Lee, Y. C. Kim, J. Seo, J. H. Noh, J. Lee and S. I. Seok, *J Am Chem Soc*, 2014, **136**, 7837-7840.
10 10.W. H. Nguyen, C. D. Bailie, E. L. Unger and M. D. McGehee, *J Am Chem Soc*, 2014, **136**, 10996-11001.
11 11.Z. Hawash, L. K. Ono, S. R. Raga, M. V. Lee and Y. Qi, *Chemistry of Materials*, 2015, **27**, 562-569.
12 12.S. Ito, S. Tanaka, H. Vahlman, H. Nishino, K. Manabe and P. Lund, *ChemPhysChem*, 2014, **15**, 1194-1200.
13 13.P. Qin, S. Tanaka, S. Ito, N. Tetreault, K. Manabe, H. Nishino, M. K. Nazeeruddin and M. Gratzel, *Nat Commun*, 2014, **5**, 3834-3840.
14 14.J. J. Shi, J. Dong, S. T. Lv, Y. Z. Xu, L. F. Zhu, J. Y. Xiao, X. Xu, H. J. Wu, D. M. Li, Y. H. Luo and Q. B. Meng, *Applied Physics Letters*, 2014, **104**, 063901-063905.
15 15.S. Aharon, S. Gamliel, B. E. Cohen and L. Etgar, *Phys Chem Chem Phys*, 2014, **16**, 10512-10518.
16 16.W. A. Laban and L. Etgar, *Energy & Environmental Science*, 2013, **6**, 3249-3253.
17 17.Z. Wei, H. Chen, K. Yan and S. Yang, *Angew Chem Int Ed Engl*, 2014, **53**, 13239-13243.
18 18.Z. Wei, K. Yan, H. Chen, Y. Yi, T. Zhang, X. Long, J. Li, L. Zhang, J. Wang and S. Yang, *Energy Environ. Sci.*, 2014, **7**, 3326-3333.
19 19.K. Yan, Z. Wei, J. Li, H. Chen, Y. Yi, X. Zheng, X. Long, Z. Wang, J. Wang, J. Xu and S. Yang, *Small*, 2015, **11**, 2269-2274.
20 20.F. Zhang, X. Yang, H. Wang, M. Cheng, J. Zhao and L. Sun, *ACS Appl Mater Interfaces*, 2014, **6**, 16140-16146.
21 21.Y. Y. Yang, J. Y. Xiao, H. Y. Wei, L. F. Zhu, D. M. Li, Y. H. Luo, H. J. Wu and Q. B. Meng, *Rsc Advances*, 2014, **4**, 52825-52830.
22 22.L. Zhang, T. Liu, L. Liu, M. Hu, Y. Yang, A. Mei and H. Han, *J. Mater. Chem. A*, 2015, **3**, 9165-9170.
23 23.H. Wei, J. Xiao, Y. Yang, S. Lv, J. Shi, X. Xu, J. Dong, Y. Luo, D. Li and Q. Meng, *Carbon*, 2015, **93**, 861-868.
24 24.A. Mei, X. Li, L. Liu, Z. Ku, T. Liu, Y. Rong, M. Xu, M. Hu, J. Chen, Y. Yang, M. Grätzel and H. Han, *Science*, 2014, **345**, 295-298.
25 25.L. Liu, A. Mei, T. Liu, P. Jiang, Y. Sheng, L. Zhang and H. Han, *J Am Chem Soc*, 2015, **137**, 1790-1793.
26 26.Z. Li, S. A. Kulkarni, P. P. Boix, E. Shi, A. Cao, K. Fu, S. K. Batabyal, J. Zhang, Q. Xiong, L. H. Wong, N. Mathews and S. G. Mhaisalkar, *ACS Nano*, 2014, **8**, 6797-6804.
27 27.S. N. Habisreutinger, T. Leijtens, G. E. Eperon, S. D. Stranks, R. J. Nicholas and H. J. Snaith, *Nano Lett*, 2014, **14**, 5561-5568.
28 28.H. Chen, Z. Wei, K. Yan, Y. Yi, J. Wang and S. Yang, *Faraday Discuss*, 2015, **176**, 271-286.
29 29.F. Xia, Q. Wu, P. Zhou, Y. Li, X. Chen, Q. Liu, J. Zhu, S. Dai, Y. Lu and S. Yang, *ACS Appl Mater Interfaces*, 2015, **7**, 13659-13665.
30 30.X. Xu, Z. Liu, Z. Zuo, M. Zhang, Z. Zhao, Y. Shen, H. Zhou, Q. Chen, Y. Yang and M. Wang, *Nano Lett*, 2015, **15**, 2402-2408.
31 31.Y. Shao, Z. Xiao, C. Bi, Y. Yuan and J. Huang, *Nat Commun*, 2014, **5**, 5784.
32 32.H.-S. Kim and N.-G. Park, *The Journal of Physical Chemistry Letters*, 2014, 2927-2934.

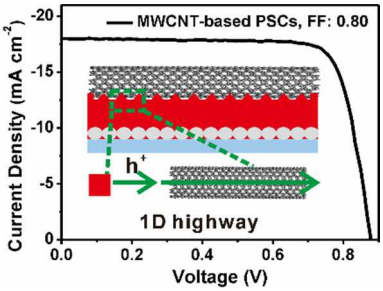

Multi-walled carbon nanotubes enable fast charge transfer in perovskite solar cells and work up a high fill factor.